Numerical Study on the Behavior of an Oscillating Wave Surge Converter

Huifeng Yu[#1], Yongliang Zhang[#2]

[#]*Department of Hydraulic Engineering, State Key Laboratory for Hydroscience and Engineering, Tsinghua University, Beijing 100084, China*

[1]yhf13@mails.tsinghua.edu.cn

[2]yongliangzhang@tsinghua.edu.cn

***Abstract*— A mathematical model is presented for the performance of an oscillating wave surge converter with a linear electric generator. The model is based on the equivalent electric circuit theory. Equations of pitch motion for the oscillating wave surge converter and a conversion relation between hydrodynamic parameters and their electrical equivalents are employed and a series electric circuit as an adjustable load of the generator is introduced, which give rise to coupled second-order ordinary differential equations governing electric current and voltage drop. The performance of the oscillating wave surge converter is investigated under three load and restriction conditions. The effects of wave frequency on capture width ratio, rotation angle complex amplitude modulus, average absorbed power and electric current phase are examined and the great benefits of a control system are demonstrated. The working process and working principle of the control system and the effect of maximum rotation angle are investigated.**

***Keywords*— Control system; equivalent electric circuit; hydrodynamic performance; linear electric generator; oscillating wave surge converter**

I. INTRODUCTION

Ocean waves are a largely untapped green renewable energy resource [1] with the highest energy flux density among all sources of renewable energy [2]. Many technologies for harvesting wave energy have been proposed over the past decades and over 6400 wave energy conversion techniques have been patented by searching the Patent Cloud. Among all kinds of devices proposed, oscillating wave surge converters (OWSCs) which basically work on the shore or in the near-shore waters have simple and reliable structures and are easy to construct and maintain [3]. Therefore, the studies of OWSCs have attracted the attention of many researchers. The representative OWSCs include Oyster, WaveRoller, EB Frond and so on [4]. The Oyster, as shown in Fig. 1a, mainly consists of a large buoyant bottom-hinged surface-piercing oscillator and two hydraulic power take-off (PTO) system located to the side of the oscillator [5]. The WaveRoller, as shown in Fig. 1b, is another advanced OWSC comprising a submerged flap attached via a pivot to a basement structure and foundation template on the seabed [6]. The EB Frond, as shown in Fig. 1c, is a submerged wave generator with a collector vane at the top of an arm pivoted near the seabed [7].

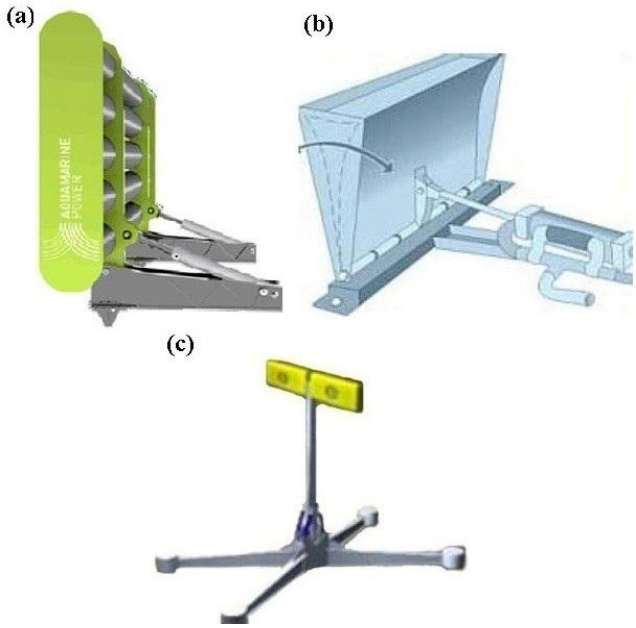

Fig. 1 Representative OWSCs: (a) Oyster; (b) WaveRoller; (c) EB Frond

Each OWSC above uses a hydraulic system as its PTO system which cannot convert its mechanical energy into electric energy directly and causes energy loss. To overcome this shortage, direct drive PTO systems, which directly convert mechanical energy of prime mover into electrical energy via linear electric generators, have been proposed as a viable alternative [8] and realized in several wave energy concepts [9]-[10]. As far as the authors are concerned, the direct drive PTO system has not been realized in an OWSC so far. Therefore, an OWSC with a linear electric generator as its direct drive PTO system is proposed. In addition, for wave energy converters (WECs), optimum control is also a very effective way to improve wave energy absorption. Control methods can be classified into continuous control method and discrete control method. The former method usually refers to phase and amplitude control whereas the latter usually refers to latching control [11]. Banks et al. [12] designed and built a Programmable Logic Controller (PLC) coupled Force Feedback Dynamometer and used it to investigate control strategies applicable to an OWSC through a variable PTO damping torque. This paper realizes continuous control by introducing an RLC series electric circuit as an adjustable load

of the generator which could act as a control system to optimize energy conversion.

The hydrodynamic characteristics of offshore structures are of significant importance [13] and much effort has been made to investigate the interactions between wave and structures [14]. In order to conveniently simulate the interactions among wave, the OWSC, the linear electric generator and the load simultaneously, we employ an equivalent circuit technique as a bridge for connecting hydrodynamic and electrical circuit problems. This equivalent circuit technique is not a new concept in structure modelling and has been applied in many aspects, such as structural mechanics problems [15], control strategy study for point absorbing WECs [16]-[19], point absorbing WEC modelling [20]-[21] and improvement of the understanding towards point absorbing WECs [22]. Shek et al. [16]-[17] presented a reaction force control scheme to maximize energy extraction of a linear electric generator for a direct drive WEC, and the equivalent circuit technique was adopted in modeling the problem. Tedeschi et al. [18] used the equivalent circuit technique to investigate the effect of control strategies on the power capture from sea waves by a point absorbing WEC. Li et al. [19] represented a point absorbing WEC by an RLC circuit and examined reactive control of the WEC to extract power in irregular waves. Hai et al. [20]-[21] established an equivalent circuit model for a point absorbing WEC and examined the accuracy of applying the model on the WEC design and performance evaluation. To the best knowledge of the authors, there is no theoretical study on an OWSC by using the equivalent electric circuit theory, especially an OWSC with a linear electric generator and control system.

This paper extends the previously mentioned modelling technique for WECs utilizing the equivalent electric circuit theory, discussed by Hai et al. [21], by considering pitch motion and an adjustable load connected to the generator as a control system, which is the first time to control an OWSC by RLC series electric circuit. The aim is to overcome the limited applicability of the technique by developing a new modelling method. By using the equivalent circuit theory, a mathematical model for analyzing wave power harvested by the OWSC with a linear electric generator is established, which is capable of quickly assessing the performance of the OWSC. In the model coupled second-order ordinary differential equations (ODEs) governing electric current and voltage drop are discretized using the fourth-order Runge-Kutta method and the integral equations for hydrodynamic parameters embedded in these ODEs are discretized using BEM. The performance of the OWSC in regular waves is analyzed under three conditions (viz., without load, with optimal load but without max rotation angle restriction and with both optimal load and maximum rotation angle restriction); particular attention is given to the influence of wave frequency on capture width ratio, rotation angle complex amplitude modulus, average absorbed power and electric current phase. The working process of the control system and the effect of maximum rotation angle are also highlighted.

II. Electric Circuit Model

Consider an OWSC with a flap and a linear electric generator as its PTO system, as shown in Fig. 2. The flap is hinged at a reinforced concrete foundation the surface of which is the same plane as the seabed. The upper part of the flap above still water level is composed of light material whose mass can be ignored whereas its lower part below still water level has uniform mass distribution. The upper and lower ends of the linear electric generator are hinged on the back of the flap and the reinforced concrete foundation, respectively. The linear electric generator mainly consists of piston cylinder, stator and translator. Part of the linear electric generator is enlarged and shown in the blue dashed box of Fig. 2. The stator is fixed inside the cylinder block and the translator is installed on the piston rod. The hydrodynamic problem of the OWSC can be formulated in a Cartesian coordinate (x,y,z) system with origin O coincident with the rotation axis centre of the flap, where the x- and y-axes are taken along the direction of wave propagation and the rotation axis of the flap, respectively, while the z-axis is in the vertical upward direction. Incident wave, the direction of which is perpendicular to the rotation axis, drives the flap to rotate around the y-axis of the hinge. The wave-induced rotation is resisted by the linear electric generator to achieve wave energy absorption. It is assumed that the flap is considered as a rigid body, the fluid is incompressible and inviscid and the flow is irrotational.

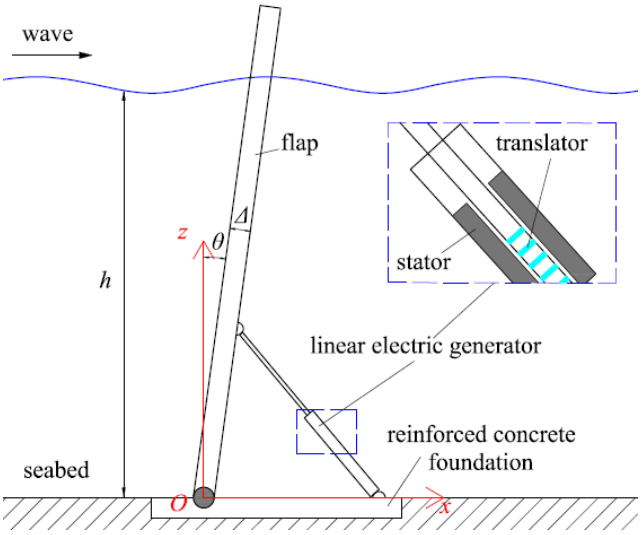

Fig. 2 Sketch of the OWSC with a linear electric generator

A. Motion Equation

In time domain, the motion of the OWSC can be described by [23]

$$\left(J+J_{\mathrm{a}}^{\infty}\right)\ddot{\theta}(t)+\int_{-\infty}^{t} f_{\mathrm{r}}(t-\tau)\dot{\theta}(\tau)\,\mathrm{d}\tau+K_{\mathrm{s}}\theta(t)+M_{\mathrm{g}}(t) =\int_{-\infty}^{\infty}\eta_{\mathrm{w}}(\tau)f_{\mathrm{e}}(t-\tau)\,\mathrm{d}\tau \tag{1}$$

where J is the rotary inertia about the y-axis of the hinge; J_{a}^{∞} is the hydrodynamic added rotary inertia at infinite frequency about the y-axis of the hinge; f_{r} is the radiation impulse-

response function (IRF); K_s is the hydrostatic restoring coefficient of pitching motion; M_g is the resistance moment induced by the linear electric generator; η_w is the water surface elevation; f_e is the excitation IRF; θ, $\dot{\theta}$ and $\ddot{\theta}$ are the rotation angle, angular velocity and the angular acceleration, respectively; t and τ are time, respectively.

The rotary inertia about the y-axis of the hinge J is

$$J = \rho_f \Delta h W \left(\Delta^2 + 4h^2\right)/12 \tag{2}$$

where ρ_f is the flap density except its upper part; Δ is the flap thickness; h is the water depth; W is the flap width.

The hydrostatic restoring coefficient of pitch motion K_s can be expressed as [24]

$$K_s = \rho g \Delta^3 W/12 + \left(\rho - \rho_f\right) g \Delta h^2 W/2 \tag{3}$$

where ρ is the seawater density; g is the gravitational acceleration.

The resistance moment induced by the linear electric generator M_g can be calculated by

$$M_g = B_g \dot{\theta} + K_g \theta \tag{4}$$

where B_g and K_g are the equivalent damping coefficient and the equivalent stiffness coefficient of the linear electric generator, respectively.

The radiation IRF f_r can be calculated through the hydrodynamic damping coefficient in frequency domain B_d [25]

$$f_r(t) = 2\int_0^\infty B_d(\omega)\cos(\omega t)\mathrm{d}\omega/\pi \tag{5}$$

where ω is the wave frequency.

The excitation IRF f_e can be calculated through the excitation moment complex amplitude in frequency domain $\hat{M}_e(\omega)$ [26]

$$f_e(t) = \int_{-\infty}^{\infty} \hat{M}_e(\omega)\mathrm{e}^{\mathrm{i}\omega t}\mathrm{d}\omega/(2\pi A) \tag{6}$$

where i is the imaginary unit; A is the wave amplitude.

The hydrodynamic added rotary inertia at infinite frequency about the y-axis of the hinge J_a^∞ has the following relation

$$J_a^\infty = \lim_{\omega\to\infty} J_a(\omega) \tag{7}$$

where J_a is the hydrodynamic added rotary inertia about the y-axis of the hinge.

The hydrodynamic parameters J_a, $\hat{M}_e$ and B_d can be calculated by the integral equations [27]

$$\begin{cases} \hat{M}_e = -\mathrm{i}\omega\rho\iint_S(\varphi_I + \varphi_D)n_5\mathrm{d}S \\ J_a = -\rho\iint_S \mathrm{Re}(\varphi_p)n_5\mathrm{d}S \\ B_d = -\omega\rho\iint_S \mathrm{Im}(\varphi_p)n_5\mathrm{d}S \end{cases} \tag{8}$$

where φ_I and φ_D are the spatial velocity potentials of incident wave and diffraction wave, respectively; φ_p is the spatial radiation potential of pitch motion with unit motion amplitude; n_5 represents the mode of pitch motion; S is the wetted surface of the flap.

When the OWSC moves in monochromatic harmonic waves, its motion equation in frequency domain is as follow

$$\begin{aligned} &\left[J + J_a(\omega)\right]\hat{\ddot{\theta}}(\omega) + \left[B_d(\omega) + B_g\right]\hat{\dot{\theta}}(\omega) \\ &+ \left(K_s + K_g\right)\hat{\theta}(\omega) = \hat{M}_e(\omega) \end{aligned} \tag{9}$$

where $\hat{\theta}$, $\hat{\dot{\theta}}$ and $\hat{\ddot{\theta}}$ are the complex amplitudes of rotation angle, angular velocity and angular acceleration, respectively.

The water surface elevation η_w of a regular wave is

$$\eta_w(t) = \mathrm{Re}\left(A\mathrm{e}^{-\mathrm{i}\omega t}\right) \tag{10}$$

Then the excitation moment M_e is

$$M_e(t) = \mathrm{Re}\left(\hat{M}_e\mathrm{e}^{-\mathrm{i}\omega t}\right) = \left|\hat{M}_e\right|\cos\left(\phi_M - \omega t\right) \tag{11}$$

where ϕ_M is the initial phase of excitation moment complex amplitude.

And the rotation angle θ is

$$\theta(t) = \mathrm{Re}\left(\hat{\theta}\mathrm{e}^{-\mathrm{i}\omega t}\right) = \left|\hat{\theta}\right|\cos\left(\phi_\theta - \omega t\right) \tag{12}$$

where ϕ_θ is the initial phase of rotation angle complex amplitude; the absolute value of θ should not exceed the maximum rotation angle θ_m.

B. Circuit Diagram

In order to derive an equivalent electric circuit from the motion equation, each physical quantity in the motion equation needs to be converted into an electrical component. Let the moment and angular velocity be equivalent to the voltage drop and electric current, respectively, then other physical quantities can be converted into corresponding electrical components according to the Ohm's law. The conversion relations have been summarized in Table I.

TABLE I
CONVERSION RELATIONS FROM PHYSICAL QUANTITIES TO ELECTRICAL COMPONENTS

Physical quantity	Circuit relation	Equivalence
$\hat{M}_e$	$\hat{U}_{AC}$	$\hat{M}_e \leftrightarrow \hat{U}_{AC}$
$\hat{\dot{\theta}}$	$\hat{I}$	$\hat{\dot{\theta}} \leftrightarrow \hat{I}$
$B\hat{\dot{\theta}}$	$\hat{U}_R = R\hat{I}$	$B \leftrightarrow R$
$K\hat{\theta} = K\hat{\dot{\theta}}/(-\mathrm{i}\omega)$	$\hat{U}_C = \hat{I}/(-\mathrm{i}\omega C)$	$1/K \leftrightarrow C$
$J\hat{\ddot{\theta}} = -\mathrm{i}\omega J\hat{\dot{\theta}}$	$\hat{U}_L = -\mathrm{i}\omega L\hat{I}$	$J \leftrightarrow L$

In Table I, $\hat{U}_{AC}$, $\hat{U}_R$, $\hat{U}_C$ and $\hat{U}_L$ are the complex amplitudes of AC voltage, resistor voltage, capacitor voltage and inductor voltage, respectively. $\hat{I}$ is the complex amplitude of electric current; R, C and L are resistance, capacitance and inductance, respectively. It can be seen that the terms that contain $\hat{\theta}$, $\hat{\dot{\theta}}$ and $\hat{\ddot{\theta}}$ can be converted into a capacitor, a resistor and an inductor, respectively. In addition, It should be pointed out that the above conversion relations are also suitable for physical quantities in real number form, such as the electric current I, the AC voltage U_{AC} and the capacitor voltage U_C. On the basis of the conversion relations, an equivalent electric circuit is derived from the OWSC motion equation, as illustrated in Fig. 3. An ampere meter is

placed in the electric circuit to measure the angular velocity of the flap.

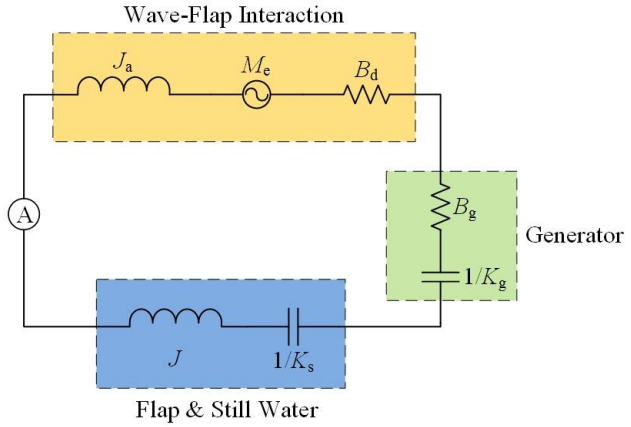

Fig. 3 Equivalent electric circuit for the OWSC

From the equivalent electric circuit model, the equivalent damping coefficient B_g of the linear electric generator is a resistor and the angular velocity is the electric current. Hence, by reading the power consumption on the resistor, it is straightforward to obtain how much active power is absorbed by the OWSC

$$P = B_g \dot{\theta}^2 \tag{13}$$

C. Load and Control

Once employing the OWSC for a certain wave frequency, e.g., ω = 0.628rad/s, the generator and flap can be optimized. Nevertheless, wave condition changes constantly in the real sea and the OWSC should adapt to these wave changes in order to achieve the maximum energy conversion. For this, an adjustable load, viz., an RLC series electric circuit, is connected to the generator as the control system and to control the OWSC. The equivalent electric circuit for the OWSC with the load is also derived, as illustrated in Fig. 4. Besides the ampere meter, one voltage meter, whose internal impedance is infinite, is placed in the electric circuit to measure the resistance moment induced by the resistors of the linear electric generator and the load. For consistency, the equivalent damping and stiffness coefficients of the linear electric generator B_g and K_g are replaced by R_g and $1/C_g$. The resistance, capacitance and inductance of the load are R_l, C_l and L_l, respectively.

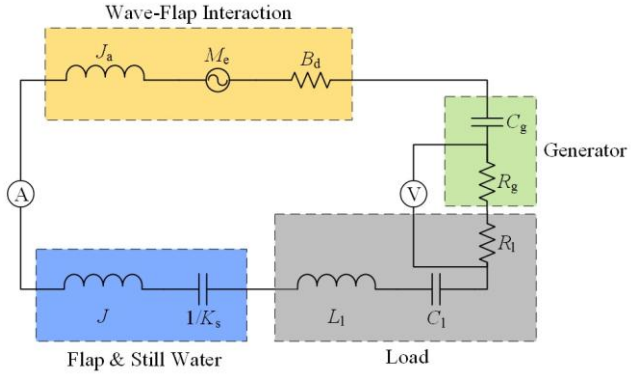

Fig. 4 Equivalent electric circuit for the OWSC with a load

When the control system is applied, the active power is

$$P = \left(R_g + R_l\right) I^2 \tag{14}$$

The circuit equations for the equivalent electric circuit can be expressed as

$$\begin{cases} \dfrac{J + J_a + L_l}{K_s + C_g^{-1} + C_l^{-1}} \ddot{U}_C + \dfrac{B_d + R_g + R_l}{K_s + C_g^{-1} + C_l^{-1}} \dot{U}_C + U_C = U_{AC} \\ I = \dot{U}_C / \left(K_s + C_g^{-1} + C_l^{-1}\right) \end{cases} \tag{15}$$

D. Parameter Determination

According to the linear wave theory, the incoming wave power per unit width of the wave front P_{in} can be expressed as

$$P_{in} = \rho g A^2 \omega \left[1 + 2kh / \sinh\left(2kh\right)\right] / 4k \tag{16}$$

where k is the wave number.

The average absorbed power over one wave period is half of the maximum absorbed power for a monochromatic harmonic wave

$$P_{avg} = P_{max} / 2 = \left(R_g + R_l\right) \left|\hat{I}\right|^2 / 2 \tag{17}$$

Then the wave energy capture width ratio can be defined as

$$\eta = P_{avg} / \left(P_{in} W\right) \tag{18}$$

For a specific OWSC, the values of J and $1/K_s$ are fixed, according to Eqs (2) and (3). Components in the Wave-Flap Interaction module, viz., J_a, M_e and B_d vary with sea states. C_g and R_g in the Generator module are fixed once upon determining their values under the given wave condition. The values of control components in the Load module need to be determined based on sea state.

According to the equivalent electric circuit for the OWSC with a load, the electric current (equivalent to the angular velocity) complex amplitude is

$$\begin{aligned} \hat{I} = \hat{M}_e / \Big[& B_d + R_g + R_l + \mathrm{i}\omega^{-1}\left(K_s + C_g^{-1} + C_l^{-1}\right) \\ & - \mathrm{i}\omega\left(J + J_a + L_l\right) \Big] \end{aligned} \tag{19}$$

Thus the average absorbed power can be expressed as

$$\begin{aligned} P_{avg} = & \frac{1}{2}\left(R_g + R_l\right) \left|\hat{M}_e\right|^2 / \Big\{ \left(B_d + R_g + R_l\right)^2 \\ & + \left[\omega^{-1}\left(K_s + C_g^{-1} + C_l^{-1}\right) - \omega\left(J + J_a + L_l\right)\right]^2 \Big\} \end{aligned} \tag{20}$$

And in an arbitrary wave frequency, take into account the load, to make the absorbed power maximum, the following relations need to be satisfied

$$\begin{cases} C_l(\omega) = \left\{\omega^2 \left[J + J_a(\omega) + L_l(\omega)\right] - K_s - C_g^{-1}\right\}^{-1} \\ R_l(\omega) = B_d(\omega) - R_g \end{cases} \tag{21}$$

However, it can be easily seen that $R_l(\omega)$ will be negative when $B_d(\omega)$ is less than R_g. Therefore, when the OWSC is connected to the load, C_g is made to be infinite (i.e., K_g = 0) and R_g is made to be zero. With regard to C_l and L_l, L_l is always made to be zero unless the corresponding C_l is negative in which case C_l is made to be infinite. The

maximum average absorbed power under the condition of optimal parameters is

$$P_{\text{avg, max}} = \left|\hat{M}_{\text{e}}\right|^2 / (8B_{\text{d}}) \tag{22}$$

III. Numerical Method

A. Circuit Equations

The coupled second-order ordinary differential equations (ODEs), viz. Eq. (15), can be solved by the fourth-order Runge-Kutta method [28]. Once the values of I and U_{C} at the n-th time step are known, we can get their values at the n+1-th step by the following equations

$$\begin{cases} I^{(n+1)} = I^{(n)} + \left(k_{1,1} + 2k_{2,1} + 2k_{3,1} + k_{4,1}\right)\Delta t / 6 \\ U_{\text{C}}^{(n+1)} = U_{\text{C}}^{(n)} + \left(k_{1,2} + 2k_{2,2} + 2k_{3,2} + k_{4,2}\right)\Delta t / 6 \\ t^{(n+1)} = t^{(n)} + \Delta t \end{cases} \tag{23}$$

where the superscripts (n) and (n+1) represent the n-th and the n+1-th time steps, respectively; Δt represents the time step; $k_{1,i}, k_{2,i}, k_{3,i}, k_{4,i}\ (i = 1, 2)$ are as follows

$$\begin{cases} k_{1,1} = \dot{I}^{(n)} = \left[U_{\text{AC}}^{(n)} - U_{\text{C}}^{(n)} - \left(B_{\text{d}} + R_{\text{g}} + R_{\text{l}}\right) I^{(n)}\right] / \\ \qquad \left(J + J_{\text{a}} + L_{\text{l}}\right) = f_1\left(t^{(n)}, I^{(n)}, U_{\text{C}}^{(n)}\right) \\ k_{1,2} = \dot{U}_{\text{C}}^{(n)} = \left(K_{\text{s}} + C_{\text{g}}^{-1} + C_{\text{l}}^{-1}\right) I^{(n)} = f_2\left(t^{(n)}, I^{(n)}, U_{\text{C}}^{(n)}\right) \\ k_{2,i} = f_i\left(t^{(n)} + \Delta t/2, I^{(n)} + k_{1,1}\Delta t/2, U_{\text{C}}^{(n)} + k_{1,2}\Delta t/2\right) \\ k_{3,i} = f_i\left(t^{(n)} + \Delta t/2, I^{(n)} + k_{2,1}\Delta t/2, U_{\text{C}}^{(n)} + k_{2,2}\Delta t/2\right) \\ k_{4,i} = f_i\left(t^{(n)} + \Delta t, I^{(n)} + k_{3,1}\Delta t, U_{\text{C}}^{(n)} + k_{3,2}\Delta t\right) \end{cases} \tag{24}$$

B. Hydrodynamic Parameters

The integral equations Eq. (8) for hydrodynamic parameters embedded in Eq. (15) are discretized using BEM [29]

$$\begin{cases} \hat{M}_{\text{e}} = -\text{i}\omega\rho \sum_{j=1}^{N} \iint_{S_j} (\varphi_{\text{I}} + \varphi_{\text{D}}) n_5 \text{d}S \\ J_{\text{a}} = -\rho \sum_{j=1}^{N} \iint_{S_j} \text{Re}(\varphi_{\text{p}}) n_5 \text{d}S \\ B_{\text{d}} = -\omega\rho \sum_{j=1}^{N} \iint_{S_j} \text{Im}(\varphi_{\text{p}}) n_5 \text{d}S \end{cases} \tag{25}$$

where S_j is the j-th discretized surface, $j = 1, 2, ..., N$; N is the number of discretized surfaces. The spatial velocity potential of incident wave φ_{I} can be calculated by an analytic formula; while spatial velocity potentials of diffraction wave and radiation wave can be calculated by the discretized boundary integral equations

$$c_i \varphi_i = \sum_{j=1}^{N} \iint_{S_j} \left(\frac{\partial \varphi}{\partial n} \varphi^* - \varphi \frac{\partial \varphi^*}{\partial n} \right) \text{d}S \tag{26}$$

where $c_i = 1 - \theta_i / (4\pi)$, θ_i is the exterior angle of the i-th discretized surface, $i = 1, 2, ..., N$; $\varphi^* = 1/(4\pi r)$, r is the distance between the centre point of the i-th discretized surface and the integration point.

IV. Results and Discussion

Following the formulation and numerical implementation presented in the previous sections, results from the numerical solution of the equivalent electric circuit model equation are presented and discussed here. The section starts with validating the present model through the comparison of the present results with the published data in Section IV-A. Then the performance of the OWSC under three conditions is examined in Section IV-B. The effects of wave frequency on capture width ratio, rotation angle complex amplitude modulus, average absorbed power and electric current phase are given in Section IV-C. Lastly, the control system and the maximum rotation angle are investigated in Section IV-D.

Parameters used in this section are given in Table II, unless otherwise specified.

TABLE II
Parameters Used for Simulations

Symbol	Value (Unit)	Symbol	Value (Unit)
A	0.1 (m)	W	5 (m)
h	5 (m)	Δ	1 (m)
ρ	1023 (kgm^{-3})	ρ_{f}	300 (kgm^{-3})
g	9.81 (ms^{-2})	θ_{m}	0.5 (rad)

A. Model Validation

Calculations have been carried out to test the present model by comparison with numerical results of Zhao et al. [30] for a bottom-hinged pendulum WEC device. The device studied by Zhao et al. [30] is similar with the present OWSC, except that the PTO system installed at the hinge is not a linear electric generator. The physical and geometric parameters used here see [30].

Figure 5 shows the comparison of the present rotation angles θ calculated by the equivalent electric circuit model with ones digitized from the published data of Zhao et al. [30] for different damping coefficients B_{g}, where all the results are plotted against wave period T. It can be seen that the maximum relative difference in rotation angles between them is within 2%. Hence, there is a good agreement between the present results and the published ones [30].

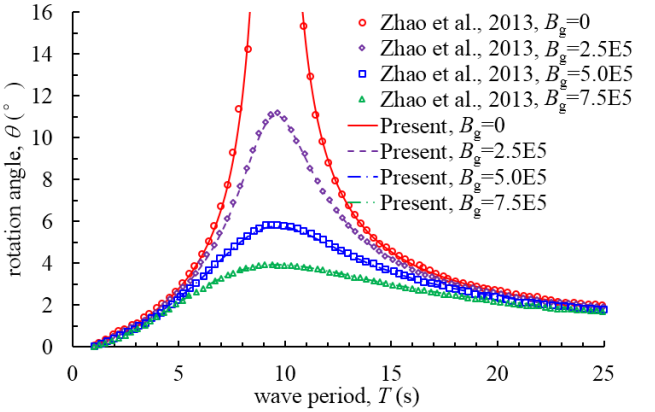

Fig. 5 Variation of θ with T for different damping coefficients B_{g}

B. *Performance under Three Conditions*

The performance of the OWSC is investigated thoroughly on the basis of the implement of equivalent electric circuit model in Matlab Simulink, as shown in Fig. 6. Figure 6a is a complete equivalent electric circuit model for the OWSC, while Fig. 6b is a simplified equivalent electric circuit model which combines all separate impedance elements into a single RLC component.

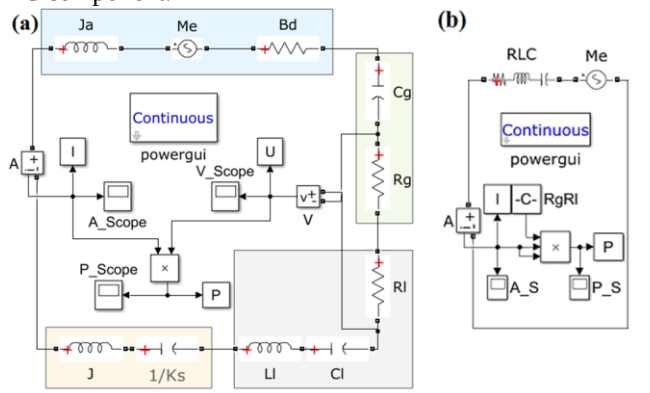

Fig. 6 Implement of equivalent electric circuit model in Matlab Simulink: (a) complete model; (b) simplified model

Figure 7 shows the variations of electric current I and excitation moment M_e with time t, respectively, for ω = 0.628rad/s and optimized linear electric generator when the load is not applied. It can be seen that there is a small phase lag of I. This is due to the fact that there is no proper C_g which can make I in phase with M_e. When I and M_e are in phase, the OWSC will resonate [27], which is an important way to improve wave energy capture. Although no resonance occurs, the capture width ratio η can still reach 175% (calculated by Eq. (18), similarly hereinafter) as the phase lag is small.

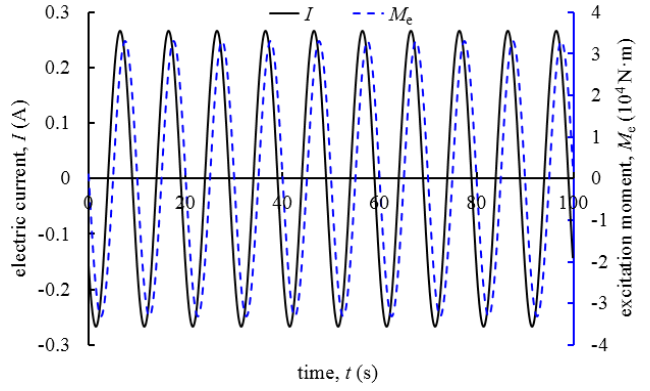

Fig. 7 Variations of I and M_e with t without load for optimal B_g and K_g

Figure 8 shows the variations of electric current I, rotation angle θ and excitation moment M_e with time t for ω = 0.628rad/s when optimal load is applied. It can be seen that I is in phase with M_e after applying optimal load. This results in the resonation of the OWSC, consequently leading an excessively large rotation angle θ (1.32rad) which may exceed the stroke of the generator. In this case, there is a need to consider applying a constraint that the rotation angle should not exceed the maximum angle θ_m. When applying the restriction of the maximum rotation angle θ_m = 0.5rad, it can be calculated that the capture width ratio η for the OWSC with optimal load is 265%, still 52% relatively larger than the capture width ratio η for the OWSC without optimal load. It should be pointed out that with the consideration of the restriction on the maximum rotation angle θ_m, we only need to appropriately increase the resistance of the load R_l so that the amplitude of rotation angle θ will reduce to θ_m while the phase of θ remains unchanged.

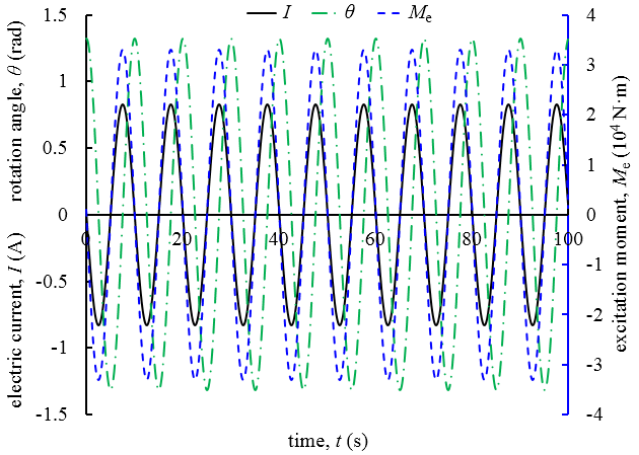

Fig. 8 Variations of I, θ and M_e with t for the OWSC with optimal load

Figure 9 shows the variations of active power absorbed by the OWSC (P) with time t for the OWSC without load, with optimal load but without restriction and with both optimal load and restriction when ω = 0.628rad/s. It can be seen that P with optimal load is in phase no matter whether the restriction is applied or not. In addition, the period of P is half of the electric current I, which can be understood according to Eq. (14), which shows that P is proportional to the square of I, and that the square of a harmonic function will halve its period. The average absorbed power P_{avg} for the OWSC with both optimal load and restriction is over 4.2kW; while the average absorbed power P_{avg} for the OWSC without load is about 2.8kW, 33% relatively smaller than that for the OWSC with both optimal load and restriction.

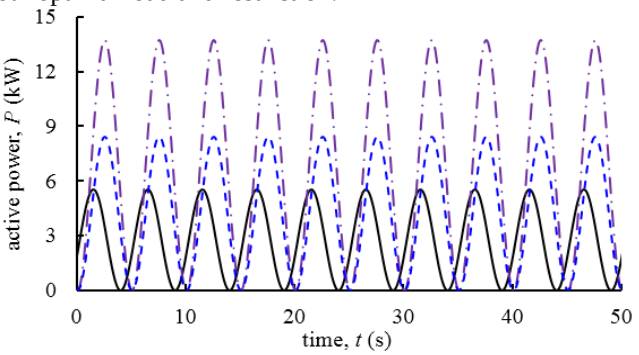

Fig. 9 Variations of P with t for different conditions: OWSC without load (solid line); OWSC with optimal load but without restriction (dash-dot line); OWSC with both optimal load and restriction (dash line)

C. *Effect of Wave Frequency*

The performance of the OWSC in terms of capture width ratio η usually is sensitive to wave frequency which always

changes constantly in the real sea. Therefore, a wide range of wave frequencies are examined to work out the effect on the performance of the OWSC.

Figures 10 and 11 show the variations of capture width ratio η and modulus of rotation angle complex amplitude $|\hat{\theta}|$ with wave frequency ω for the OWSC without load, with optimal load but without restriction and with both optimal load and restriction, respectively. It can be seen from Fig. 10 that for the OWSC without load and with both optimal load and restriction, η first increase with the increase of wave frequency ω, and then decrease after reaching a maximum value. For the OWSC with optimal load but without restriction, η monotonically decreases with the increase of wave frequency ω. η for the OWSC with both optimal load and restriction is always larger than that without load, the average capture width ratio of the former is 95%, 7.5 times as large as that of the latter; when capture width ratio is 100%, the frequency bandwidth of the former is more than 11 times larger than that of the latter. Figure 11 shows that for the OWSC without load, $|\hat{\theta}|$ first increases with the increase of wave frequency ω, and then decreases after reaching a maximum value, which occurs at ω = 0.691rad/s. For the OWSC with optimal load but without restriction, $|\hat{\theta}|$ monotonically decreases with the increase of wave frequency ω. When ω<0.817rad/s for the OWSC with optimal load but without restriction, $|\hat{\theta}|$ will be larger than the maximum rotation angle θ_m = 0.5rad, thus $|\hat{\theta}|$ is always equal to θ_m for the OWSC with both optimal load and restriction. When 1.7rad/s<ω<3.9rad/s, $|\hat{\theta}|$ for the OWSC with optimal load is smaller than that without load, although η for the OWSC with optimal load is larger than that without load.

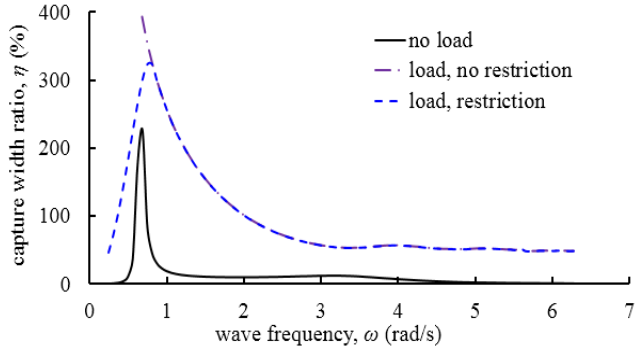

Fig. 10 Variations of η with ω for different conditions

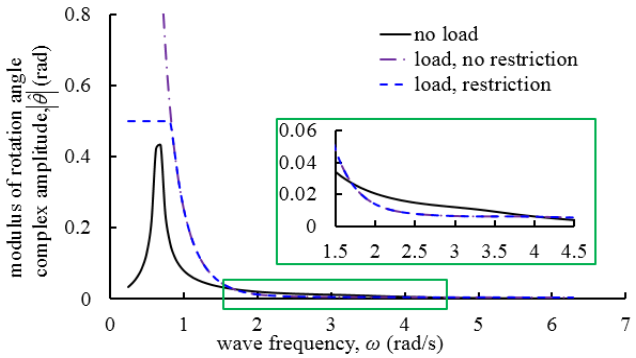

Fig. 11 Variations of $|\hat{\theta}|$ with ω for different conditions

Figure 12 shows the variations of average absorbed power P_{avg} with wave frequency ω for the OWSC without load and with both optimal load and restriction. It can be seen that P_{avg} for the OWSC with both optimal load and restriction is always larger than that without load, the maximum P_{avg} of the former is 4.9kW, 1.4 times as large as that of the latter; and comparing the frequency bandwidth when P_{avg} is 2kW, the frequency bandwidth of the former is more than 6.5 times larger than that of the latter. When optimal load and restriction are applied, the optimal wave frequency corresponding to the maximum P_{avg} is larger than the counterpart for the OWSC without load. This is due to the fact that the resonance frequency for the OWSC without load for optimal B_g and K_g is 0.691rad/s, whereas for the OWSC with both optimal load and restriction, whose optimal wave frequency equals the one that makes $|\hat{\theta}|$ just arrive θ_m, it is 0.817rad/s when θ_m = 0.5rad.

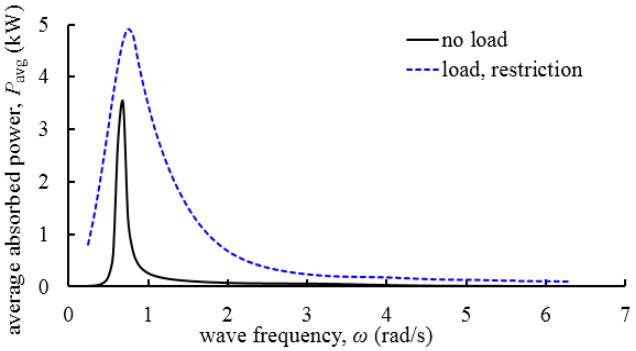

Fig. 12 Variations of P_{avg} with ω for different conditions

Figure 13 shows the variations of the phase of electric current ϕ_I with wave frequency ω for the OWSC without load and with optimal load. It can be seen that ϕ_I for the OWSC with optimal load agrees well with the phase of excitation moment ϕ_M, while there is always a large phase difference between ϕ_I for the OWSC without load and ϕ_M except when ω is close to 0.628rad/s. The phase difference here is an important factor that leads to the very small capture width ratio of the OWSC without load when ω is away from 0.628rad/s. It also can be seen from Fig. 10 that when 2rad/s<ω<3.3rad/s, η for the OWSC without load increases with increasing ω, partly due to the relative small phase difference within this range.

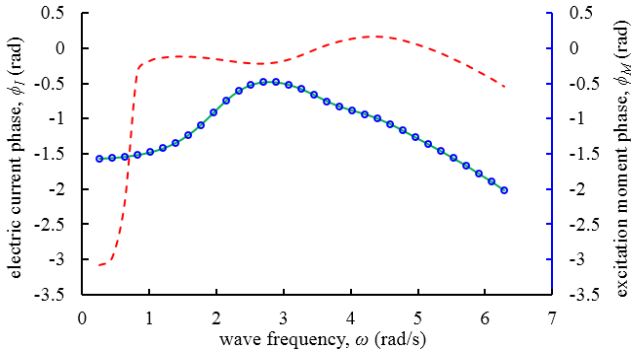

Fig. 13 Variations of ϕ_I with ω: OWSC without load (dash line); OWSC with optimal load (solid line); ϕ_M (o).

D. Control System

Control system plays a significant role in the wave energy capture, therefore this paper investigates the working process and working principle of the control system over a wide range of wave frequencies. Moreover, the effect of the maximum rotation angle θ_m on the OWSC performance and the control system is also examined here.

There are three components in the control system: load resistance R_l, load capacitance C_l and load inductance L_l. C_l and L_l are used to make the electric current I (i.e., the angular velocity $\dot{\theta}$) in phase with the excitation moment M_e, while R_l is used to control the amplitude of the rotation angle θ once upon C_l and L_l are determined. As the components need to change with wave frequency, therefore a measurement or prediction of the wave frequency is of necessity. When there is no restriction on the rotation angle θ, R_l is the same as the hydrodynamic damping coefficient B_d according to Eq. (21).

Figure 14 shows the variations of $1/C_l$ and L_l with wave frequency ω for the OWSC with optimal load. It can be seen that $1/C_l$ is always zero when ω<0.66rad/s. When ω>0.66rad/s, $1/C_l$ increases and then decreases after reaching a peak value, and then increases monotonically after reaching a valley value. On the whole $1/C_l$ increases with ω while L_l is contrary to $1/C_l$. It should be pointed out that for realistic capacitor and inductor, it is impossible to make C_l and L_l very large, thus some range of wave frequencies are beyond control capability. The change trend of either $1/C_l$ or L_l with wave frequency does not change with or without restriction on the rotation angle θ.

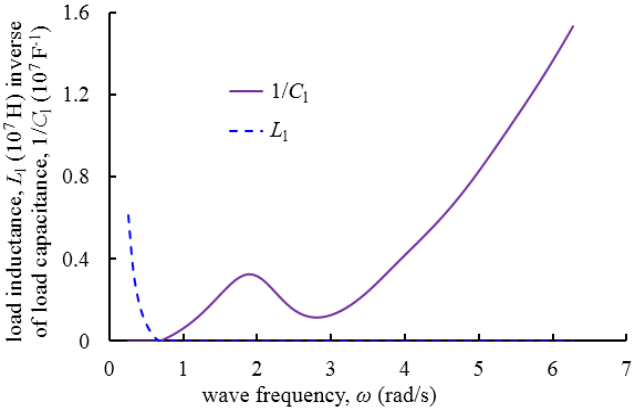

Fig. 14 Variations of $1/C_l$ and L_l with ω for the OWSC with optimal load

Figure 15 shows the variations of R_l with wave frequency ω for the OWSC with optimal load for five restriction conditions in terms of maximum rotation angles θ_m. It can be seen that generally the smaller θ_m is, the bigger R_l is needed and the less the overlap part between each curve for the OWSC with optimal load and restriction and the curve for no restriction is. R_l value corresponding to the starting point of each overlap part increases with decreasing θ_m.

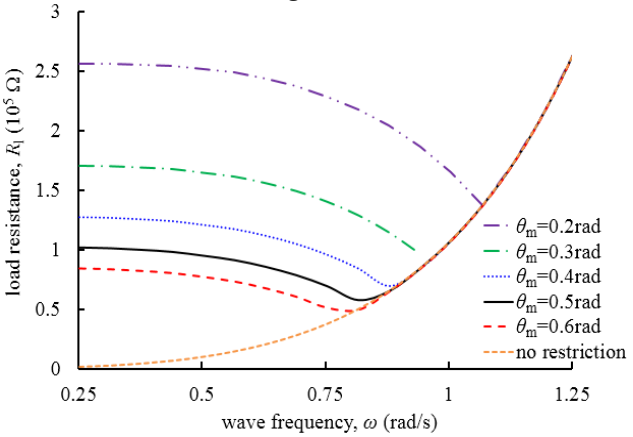

Fig. 15 Variations of R_l with ω for the OWSC with optimal load for five θ_m

Figure 16 shows the variations of capture width ratio η with wave frequency ω for the OWSC with optimal load for five maximum rotation angles θ_m. It can be seen that the smaller θ_m is, the smaller η is and the less the overlap part between each curve for the OWSC with optimal load and restriction and the curve for no restriction is. The wave frequency corresponding to the maximum capture width ratio decreases with the increase of the maximum rotation angles θ_m.

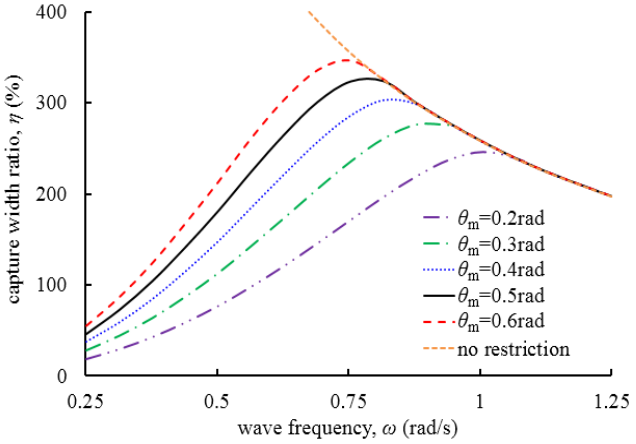

Fig. 16 Variations of η with ω for the OWSC with optimal load for five θ_m

V. Conclusions

In this paper, a mathematical model based on the equivalent electric circuit theory is presented for the performance of an OWSC with a linear electric generator. Coupled second-order ODEs governing electric current and voltage drop is obtained by using the equations of pitch motion for the OWSC and a conversion relation between hydrodynamic parameters and

their electrical equivalents, and introducing an RLC series electric circuit as an adjustable load of the generator. These ODEs are discretized using the fourth-order Runge-Kutta method and the integral equations for hydrodynamic parameters embedded in these ODEs are discretized using BEM. Then the performance of the OWSC in regular waves is investigated.

We have found that when there is no load, the OWSC is unable to achieve resonation for the examined conditions. Once optimal load is applied, leading to the occurance of resonance of the OWSC, the capture width ratio can reach 265% when a maximum rotation angle is taken into consideration, 52% relatively larger than that of the OWSC without load. It is also revealed that for the OWSC without load and with both optimal load and restriction, the capture width ratio first increase with increasing wave frequency, and then decrease after reaching a maximum value; while for the OWSC with optimal load but without restriction, the capture width ratio monotonically decreases with increasing wave frequency. The average capture width ratio for the OWSC with both optimal load and restriction is 95%, 7.5 times as large as that for the OWSC without load. When capture width ratio is 100%, the frequency bandwidth of the former is more than 11 times larger than that of the latter. The good performance of the former is guaranteed by the control system which always makes the equivalent damping coefficient optimized and keeps the OWSC in resonation.

The load capacitance and the load inductance in the control system are used to make the OWSC resonate, while the load resistance in the control system is used to control the amplitude of the rotation angle once upon the load capacitance and the load inductance are determined. With regard to the maximum rotation angle, the smaller it is, the bigger the load resistance is needed, the smaller the capture width ratio is and the less the overlap part between each R_l~ω curve for the OWSC with optimal load and restriction and the R_l~ω curve for no restriction is.

Being the first time to use equivalent electric circuit theory into modelling an OWSC, many advantages can be discovered. By converting hydrodynamic parameters into electrical components, the electric circuit model promotes the understanding of the relations among each element of the OWSC, especially for those who are not familiar with hydrodynamic simulation. The electric circuit model can be extended easily and is able to analyse an OWSC array. Moreover, the electric circuit model provides a method to assess the performance of an OWSC quickly.

Future work will focus on the further validation of the electric circuit model via physical experiments and taking system friction and dead zone into consideration to make the simulation more realistic.

ACKNOWLEDGMENT

The research was supported by the National Natural Science Foundation of China [grant 51479092, grant 51679124].

REFERENCES

[1] K. Gunn, and C. Stock-Williams, "Quantifying the global wave power resource," *Renewable Energy*, vol. 44, no. 4, pp. 296-304, Aug. 2012.

[2] A. Cl ément, P. Mccullen, A. Falc ão, A. Fiorentino, F. Gardner, K. Hammarlund, G. Lemonis, T. Lewis, K. Nielsen, S. Petroncini, M. T. Pontes, B. O. Schild, P. Sj östr öm, H. C. S ørresen and T. Thorpe, "Wave energy in Europe: current status and perspectives," *Renewable and Sustainable Energy Reviews*, vol. 6, no. 5, pp. 405-431, Jun. 2002.

[3] S. M. Zheng, and Y. L. Zhang, "Study on the wave power absorption of a raft-typed wave energy collector," *J. Eng. Heilongjiang Univ.*, vol. 5, no. 2, pp. 7-13, Jun. 2014.

[4] M. Folley, T. Whittaker, and T. H. J. Van, "The design of small seabed-mounted bottom-hinged wave energy converters," in *Proc. 7th Eur. Wave Tidal Energy Conf.*, Porto, Portugal, 2007.

[5] A. Henry, K. Doherty, L. Cameron, T. Whittaker, and R. Doherty, "Advances in the design of the Oyster wave energy converter," in *Proc. RINA Marine and Offshore Renew. Energy Conf.*, London, UK, 2010.

[6] T. Mäki, M. Vuorinen, and T. Mucha, "WaveRoller – One of the Leading Technologies for Wave Energy Conversion," in *Proc. 5th Int. Conf. Ocean Energy*, Halifax, Canada, 2014.

[7] "EB Frond wave energy converter – phase 2," The Engineering Business Ltd, UK, DTI Report URN05/865, 2005.

[8] M. A. Mueller, "Electrical generators for direct drive wave energy converters," *Generation, Transmission and Distribution, IEE Proceedings- 2002*, vol. 149, pp. 446-456, 2002.

[9] K. Rhinefrank, E. B. Agamloh, A. V. Jouanne, A. K. Wallace, J. Prudell, K. Kimble, J. Aills, E. Schmidt, P. Chan, B. Sweeny, and A. Schacher, "Novel ocean energy permanent magnet linear generator buoy," *Renewable Energy*, vol. 31, no. 9, pp. 1279-1298, Jul. 2006.

[10] J. Prudell, M. Stoddard, E. Amon, and T. K. A. Brekken, "A permanent-magnet tubular linear generator for ocean wave energy conversion," *IEEE Trans. Ind. Appl.*, vol. 46, no. 6, pp. 2392-2400, Sep. 2010.

[11] J. Falnes, "Optimum control of oscillation of wave-energy converters," *International Journal of Offshore & Polar Engineering*, vol. 12, no. 2, pp. 147-155, Jun. 2002.

[12] D. Banks, J. V. T. Hoff, and K. Doherty, "The Development of an Experimental Force Feedback Dynamometer to Investigate the Real Time Control of an Oscillating Wave Surge Converter," presented at ASME 2013 International Conference on Ocean, Offshore and Arctic Engineering, Jun. 2013.

[13] S. M. Zheng, and Y. L. Zhang, "Wave diffraction and radiation by multiple rectangular floaters," *Journal of Hydraulic Research*, vol. 54, no. 1, pp. 102-115, 2016.

[14] T. H. Koftis, P. Prinos, and E. Koutandos, "2D-V hydrodynamics of wave–floating breakwater interaction," *Journal of Hydraulic Research*, vol. 44, no. 4, pp. 451-469, 2006.

[15] A. Suat Ekinci, and A. Atalar, "An electrical circuit theoretical method for time- and frequency- domain solutions of the structural mechanics problems," *International Journal for Numerical Methods in Engineering*, vol. 45, no. 10, pp. 1485-1507, 2015.

[16] J. K. H. Shek, D. E. Macpherson, M. A. Mueller, and J. Xiang, "Reaction force control of a linear electrical generator for direct drive wave energy conversion," *Iet Renewable Power Generation*, vol. 1, no. 1, pp. 17-24, Mar. 2007.

[17] J. K. H. Shek, D. E. Macpherson, and M. A. Mueller, "Phase and amplitude control of a linear generator for wave energy conversion," presented at 4th IET International Conference on Power Electronics, Machines and Drives (PEMD 2008), Apr. 2008.

[18] E. Tedeschi, M. Carraro, M. Molinas, and P. Mattavelli, "Effect of control strategies and power take-off efficiency on the power capture from sea waves," *IEEE Trans. Energy Convers.*, vol. 26, no. 4, pp. 1088-1098, Sep. 2011.

[19] B. Li, D. E. Macpherson, and J. K. H. Shek, "Direct drive wave energy converter control in irregular waves," *Renewable Power Generation*, pp. 1-6, Sept. 2011.

[20] L. Hai, M. G öteman, and M. Leijon, "A methodology of modelling a wave power system via an equivalent RLC circuit," *IEEE Transactions on Sustainable Energy*, vol. 7, pp. 1362-1370, Oct. 2016.

[21] L. Hai, O. Svensson, J. Isberg, and M. Leijon, "Modelling a point absorbing wave energy converter by the equivalent electric circuit theory: a feasibility study," *Journal of Applied Physics*, vol. 117, pp. 899-918, Apr. 2015.

[22] T. K. A. Brekken, A. V. Jouanne, and H. Y. Han, "Ocean wave energy overview and research at Oregon State University," in *Proc. Power Electron. Mach. Wind Appl.*, Lincoln, USA, 2009, pp. 135-141.
[23] W. E. Cummins, "The impulse response function and ship motions," *Schiffstechnik*, vol. 9, pp. 101-109, Jan. 1962.
[24] H. T. Zhao, "Hydrodynamic research of a bottom-hinged flap wave energy convertor," Ph.D. dissertation, Colg. Civil Eng. Arch.., Zhejiang Univ., Hangzhou, China, 2012.
[25] W. A. Sheng, and A. Lewis, "Assessment of wave energy extraction from seas: numerical validation," *Journal of Energy Resources Technology*, vol. 134, no. 4, pp. 103-116, Aug. 2012.
[26] C. H. Lee, and J. N. Newman, "Computation of wave effects using the panel method," in *Numerical Models in Fluid-Structure Interaction*, 1st ed., S. K. Chakrabarti, Ed. Southampton, UK: WIT Press, 2005, ch. 6, pp. 211-251.
[27] J. Falnes, *Ocean waves and oscillating systems: linear interactions including wave-energy extraction*, New York, USA: Cambridge University Press, 2002.
[28] E. Süli, and D. F. Mayers, *An introduction to numerical analysis*, New York, USA: Cambridge University Press, 2003.
[29] Q. Shen, X. Chen, and Z. Jiang, *The fluid-structure interaction dynamic analysis of floating body and floating multibody system*, Beijing, China: Science Press, 2011.
[30] H. T. Zhao, Z. L. Sun, C. L. Hao, and J. F. Shen, "Numerical modeling on hydrodynamic performance of a bottom-hinged flap wave energy converter," *China Ocean Eng.*, vol. 27, no. 1, pp. 73-86, Apr. 2013.